Combining Structural with Functional Model Properties in Iron Synthetic Analogue Complexes for the Active Site in Rabbit Lipoxygenase

Dobbelaar, Emiel; Rauber, Christian; Bonck, Thorsten; Kelm, Harald; Schmitz, Markus; De Waal Malefijt, Matina Eloïse; Klein, Johannes E.M.N.; Krüger, Hans Jörg

Published in:
Journal of the American Chemical Society

DOI:
10.1021/jacs.1c04422

Publication date:
2021

JACS
JOURNAL OF THE AMERICAN CHEMICAL SOCIETY
pubs.acs.org/JACS
Article

Combining Structural with Functional Model Properties in Iron Synthetic Analogue Complexes for the Active Site in Rabbit Lipoxygenase

Emiel Dobbelaar, Christian Rauber, Thorsten Bonck, Harald Kelm, Markus Schmitz, Matina Eloïse de Waal Malefijt, Johannes E. M. N. Klein, and Hans-Jörg Krüger*

Cite This: *J. Am. Chem. Soc.* 2021, 143, 13145−13155

ABSTRACT: Iron complexes that model the structural *and* functional properties of the active iron site in rabbit lipoxygenase are described. The ligand sphere of the mononuclear pseudo-octahedral *cis*-(carboxylato)(hydroxo)iron(III) complex, which is completed by a tetraazamacrocyclic ligand, reproduces the first coordination shell of the active site in the enzyme. In addition, two corresponding iron(II) complexes are presented that differ in the coordination of a water molecule. In their structural and electronic properties, both the (hydroxo)iron(III) and the (aqua)iron(II) complex reflect well the only two essential states found in the enzymatic mechanism of peroxidation of polyunsaturated fatty acids. Furthermore, the ferric complex is shown to undergo hydrogen atom abstraction reactions with O−H and C−H bonds of suitable substrates, and the bond dissociation free energy of the coordinated water ligand of the ferrous complex is determined to be 72.4 kcal·mol^{-1}. Theoretical investigations of the reactivity support a concerted proton-coupled electron transfer mechanism in close analogy to the initial step in the enzymatic mechanism. The propensity of the (hydroxo)iron(III) complex to undergo H atom abstraction reactions is the basis for its catalytic function in the aerobic peroxidation of 2,4,6-tri(*tert*-butyl)phenol and its role as a radical initiator in the reaction of dihydroanthracene with oxygen.

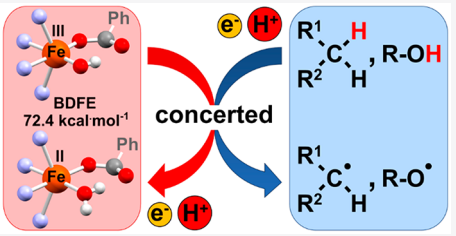

INTRODUCTION

Lipoxygenases (LOXs) are enzymes found in plants and animals that contain a mononuclear *cis*-(carboxylato)-(hydroxo)iron(III) coordination unit as the catalytically active site for the hydroperoxidation of (*Z*,*Z*)-1,4-pentadiene moieties with molecular oxygen.[1−3] These enzymes play a major role, for example, in regulating the metabolism of polyunsaturated fatty acids, such as linoleate and arachidonate, in controlling cellular differentiation and growth, and in initiating inflammatory processes in mammals.[4,5] On the basis of the structural parameters of the enzymes in the reduced *cis*-(carboxylato)(aqua)iron(II) state, the distance found between the oxygen atoms deriving from the water ligand and the carbonyl group of the carboxylate ligand (deriving from the C-terminal amino acid isoleucine) indicates the existence of a hydrogen bonding interaction between these ligands.[6] While the residual distorted octahedral coordination sphere of the active nonheme iron(III) unit is completed by four histidine nitrogen donors in rabbit and human 15-lipoxygenases (rLOXs[7,8] and hLOXs[9]), the composition of the protein-derived ligand environment in lipoxygenases from other sources varies by substitution of one of the histidine residues, e.g., by an asparagine carbonyl oxygen donor.[2,6,10−12] The most widely accepted mechanism involves two states for the iron site: a high-spin ferric hydroxide and a high-spin ferrous aqua complex (Scheme 1a).[2,13] In the initial step of the reaction cycle, the ferric hydroxide converts the pentadiene unit into a pentadienyl radical via an overall H atom abstraction (Scheme 1b).

The current state of research describes the elementary reaction step of C−H bond peroxidation as a concerted proton-coupled electron transfer (PCET).[2,14−16] After rearrangement, the pentadienyl radical formed reacts with triplet oxygen, yielding a peroxyl radical intermediate, which then abstracts a hydrogen atom from the ferrous aqua unit under regeneration of the original ferric hydroxide state.

The objective of the synthetic analogue approach (structural−functional modeling) in bioinorganic studies entails the synthesis of small inorganic model complexes that provide a rational basis to understanding the structural, electronic, or mechanistic properties of the metal sites in metalloproteins and help to identify those intrinsic properties of the enzyme associated with the metal site and its first coordination sphere and those related to the protein matrix.[17−19] In addition to the

Received: April 28, 2021
Published: August 12, 2021

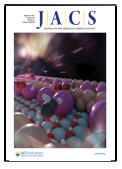

https://doi.org/10.1021/jacs.1c04422
J. Am. Chem. Soc. 2021, 143, 13145−13155

Scheme 1. (a) Iron Sites of the Enzymatic States Involved in the Catalytic Cycle; (b) Generally Accepted Radical Mechanism for the Peroxidation of the 1,4-Pentadiene Unit in Polyunsaturated Fatty Acids by rLOX

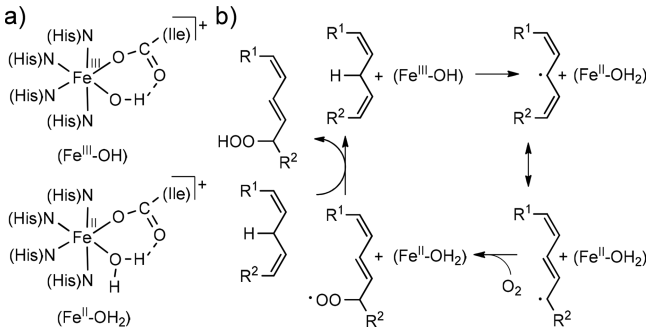

gains in knowledge of bioinorganic issues, the results of such a study could reward researchers interested in developing novel catalysts with potential information about those features, which are essential for a reactivity similar to the enzyme's.

Both functional[13,20−22] and structural[23,24] model complexes for lipoxygenases have previously been reported; however, none of these combine both structural *and* functional properties. Probably, the most challenging part of generating a structural model for the active site in rabbit lipoxygenase is the preparation of a mononuclear (hydroxo)iron(III) complex that maintains its mononuclearity in solution and does not undergo the usually observed formation of μ-oxo-bridged oligonuclear iron(III) species.[25,26] Until recently, reports of mononuclear (hydroxo)iron(III) complexes that had been structurally characterized were rare. However, an increasing number of new examples have been published over the past few years, providing evidence of a developing interest in such compounds.[23,24,27−44] Strategies to achieve mononuclearity include (i) sterically shielding the Fe^{III}OH site, (ii) increasing the electron donating capabilities of the ancillary ligand by incorporating negatively charged donor groups, (iii) increasing the coordination number of the iron(III) ion, and (iv) furnishing the ancillary ligand with hydrogen bond donors for the interaction with the electron lone pairs of the coordinated hydroxide ligand. On the basis of the results of a preliminary study on iron complexes with sterically less demanding diazapyridinophane derivatives, the tetradentate macrocyclic *N*,*N*′-di-*tert*-butyl-2,11-diaza[3.3](2,6)-pyridinophane ligand (L-N$_4^t$Bu$_2$, Scheme 2) is employed in this investigation. Upon coordination, the large *tert*-butyl substituents are located above and below the two remaining *cis*-coordination sites at the metal ion with a distorted octahedral environment, thereby preventing the formation of μ-oxo bridged dinuclear metal complexes by steric shielding.

Scheme 2. Tetradentate Macrocyclic Ligand L-N$_4^t$Bu$_2$

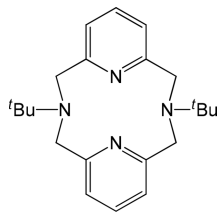

RESULTS AND DISCUSSION

Synthesis and Structural Characterization. The mononuclear (benzoato)(hydroxo)iron(III) complex [Fe(L-N$_4^t$Bu$_2$)(O$_2$CPh)(OH)]$^+$ (**1**) was obtained by the reaction of the bis(methanolato)iron(III) complex [Fe(L-N$_4^t$Bu$_2$)-(OMe)$_2$]$^+$ (**4**) with one equivalent of benzoic acid in an acetonitrile solution containing only small amounts of water. Complex **4**, in turn, is conveniently prepared from the dichloroiron(II) complex [Fe(L-N$_4^t$Bu$_2$)Cl$_2$] (**5**)[45] in methanol under aerobic conditions upon base addition. Complex **5** also serves as a starting material in the synthesis of the respective (benzoato)iron(II) complexes [Fe(L-N$_4^t$Bu$_2$)-(O$_2$CPh)(OH$_2$)]$^+$ (**2**) and [Fe(L-N$_4^t$Bu$_2$)(O$_2$CPh)]$^+$ (**3**). In alcoholic solutions, the coordinated water molecule in **2** can be replaced by a wide variety of alcohol molecules (e.g., by MeOH in [Fe(L-N$_4^t$Bu$_2$)(O$_2$CPh)(MeOH)]$^+$ (**6**)); in contrast, using anhydrous acetonitrile, complex **3** can be obtained where the benzoate unit acts as a bidentate chelating ligand. Under air, complex **2** forms complex **1**, but this reaction is not fully quantitative and is, therefore, an impractical method of obtaining complex **1** as an analytically pure material. Complex cations **1**, **2**, and **4** were isolated with a variety of counterions. The synthetic efforts, the structures of **1**, **2**, and **3**, and a list of individual analytically pure substances obtained in this study are contained in Scheme 3; synthetic details are described in the Supporting Information.

Scheme 3. (a) Synthetic Reactions and (b) Structures of 1, 2, and 3[a]

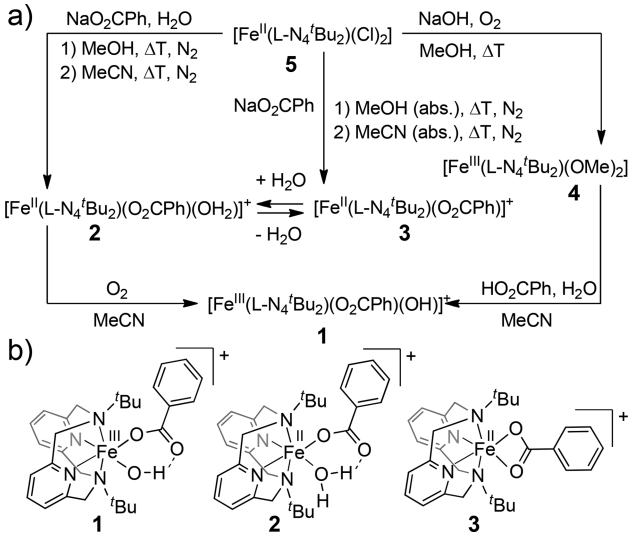

[a]The cationic complexes were crystallized and isolated as [**1**]BPh$_4$ (**1a**), [**1**]BPh$_4$·MeCN (**1b**), [**1**]PF$_6$ (**1c**), [**2**]ClO$_4$ (**2a**), [**2**]PF$_6$ (**2b**(**1**), *P*2$_1$/*n*, and **2b**(**2**), *C*2/*c*), [**2**]CF$_3$SO$_3$ (**2c**), [**3**]ClO$_4$·MeCN (**3a**), [**4**]BPh$_4$ (**4a**), and [**4**]PF$_6$ (**4b**).

All novel compounds (**1**−**4**, **6**) were structurally characterized by X-ray structure analyses. Representative perspective views of the complex cations **1**, **2**, and **3** are given in Figure 1, including the applied numbering of those atoms relevant to the subsequent discussion. Since complex cations **1** and **2** could be structurally investigated with different counterions, the measured lengths for equivalent bonds from these different structure analyses span a range. Especially, due to different hydrogen-bonding patterns of the coordinated water molecule

https://doi.org/10.1021/jacs.1c04422
J. Am. Chem. Soc. 2021, 143, 13145−13155

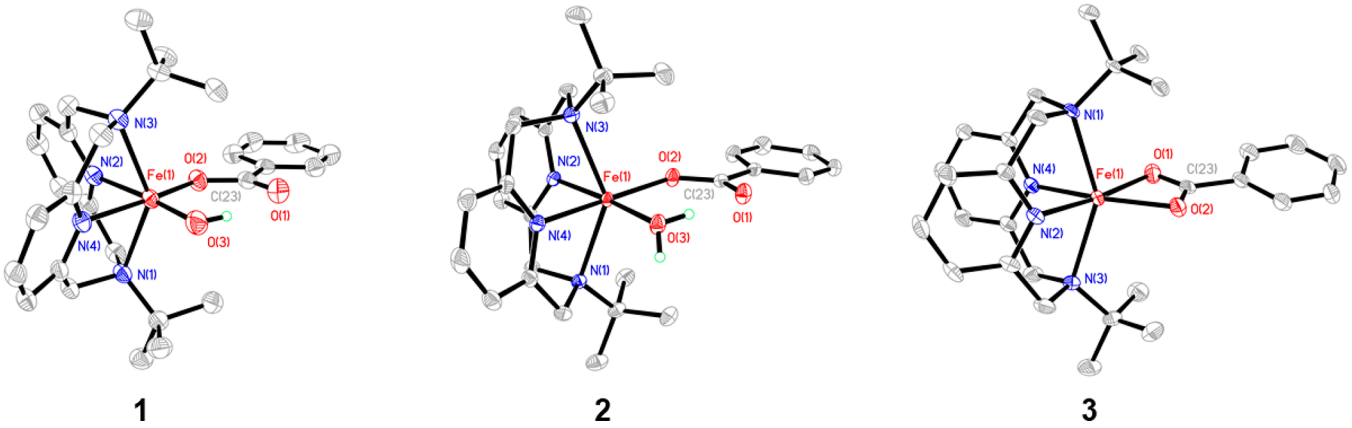

Figure 1. Perspective views of the complex cations in the ferric compound **1a**, and both ferrous compounds **2a** and **3a** with thermal ellipsoids displaying a probability level of 50%. Hydrogen atoms are omitted for clarity with the exception of those bound to O(3).

in the individual crystal packings, the spread of bond lengths in **2** is somewhat larger than that in **1**. Thus, in Table 1, the ranges of some selected bond lengths or interatomic distances and their changes between the ferric complex **1** and the ferrous complex **2** are provided. Upon coordination, the tetradentate macrocyclic ligand is folded along the N_{amine}−N_{amine} axis, leaving two *cis* coordination sites *trans* to the pyridine nitrogen donor atoms to be occupied by the two oxygen donor atoms originating from monodentate benzoate and hydroxide or water ligands in **1** or **2** and from the chelating benzoate ligand in **3**, respectively. The coordinated tetraazamacrocyclic ligand is slightly twisted, resulting in an idealized C_2-symmetry of the [Fe(L-$N_4{}^tBu_2$)] fragment. In both complexes **1** and **2**, the most noteworthy structural feature is the almost planar hexagon formed by the iron ion, the coordinated carboxylate group, the hydroxide/water ligand, and the hydrogen bonding interaction between carboxylate and hydroxide/water moieties (Tables S5 and S10). As a consequence of the prominent hydrogen bonding bridge, the lone pairs of the coordinated hydroxo ligand in **1** are oriented in such a way that a reaction path for an overall hydrogen abstraction reaction from the O−H and C−H bonds of suitable substrates is enabled while maintaining the mononuclearity of the ferric complex (Figure S27). In addition, the other hydrogen atom of the coordinated water ligand in **2** can engage in various intermolecular hydrogen bonding interactions with either the counterion or a neighboring complex cation as established by several crystal structure analyses of complexes with different counterions (Table S8).

Table 1. Selected Bond Lengths and Interatomic Distances (in Å) in the Ferric Complex Cation 1[a] and the Ferrous Complex Cations 2[b] and 3[c] and Differences (Δ*d*) in the Lengths of the Respective Bonds upon Oxidation of 2 to 1[d]

	3	2	1	Δ(*d*(**1**) − *d*(**2**))
Fe−O(2)	2.08	2.02−2.05	1.95−1.96	−(0.06−0.10)
Fe−O(3)		2.08−2.12	1.83−1.85	−(0.23−0.29)
Fe−N(1) or Fe−N(3)	2.31, 2.40	2.35−2.39	2.29−2.34	−(0.01−0.10)
Fe−N(2)	2.14	2.08−2.10	2.10−2.11	+(0−0.03)
Fe−N(4)	2.11	2.10−2.12	2.08−2.10	−(0−0.04)
Fe···O(1)	2.24	3.41−3.42	3.30−3.36	−(0.05−0.12)
O(1)···O(3)		2.58−2.63	2.79−2.96	+(0.38−0.16)

[a]From the structural analyses of **1a**, **1b**, and **1c**. [b]From the structural analyses of **2a**, **2b(1)**, **2b(2)**, and **2c**. [c]From the structural analysis of **3a**. [d]Despite the higher experimental accuracy, all bond lengths are rounded to a hundredth of an Å for clarity. N(1) and N(3) are the axial amine donors; N(2) is the pyridine nitrogen atom *trans* to the hydroxide/aqua oxygen donor O(3); N(4) is the pyridine nitrogen atom *trans* to the carboxylate oxygen donor O(2). O(1) refers to the carbonyl oxygen atom of the carboxylate ligand. For more details, see the Supporting Information.

As usually observed in pseudo-octahedral complexes with diazapyridinophane ligands, the axial Fe−N_{amine} bonds are considerably longer than the Fe−N_{py} bonds in the equatorial coordination plane of the metal ion.[45,46] The Fe−N bond lengths to the macrocyclic ligand can be used to unambiguously identify the spin state of the iron ion. The relatively long Fe−N bonds in complexes **1** and **2** are consistent with other high-spin iron complexes containing this macrocyclic ligand. The comparison of the bond lengths in complexes **1** and **2** reveals that all Fe−N/O bonds decrease in length upon oxidation except for the Fe−N_{py} bond *trans* to the hydroxide/water ligand. The reverse trend for the latter bond is related to the stronger *trans* influence of the anionic hydroxide ligand. Despite this detail, the smallest change in bond length is observed for the Fe−N_{py} bonds; the already quite elongated axial Fe−N_{amine} bonds react to the change in the oxidation state of the metal ion with a somewhat larger alteration of the bond length, probably due to the fact that these already weak axial bonds are characterized by rather soft vibration modes.

The Fe−O bonds to the carboxylate and especially to the water/hydroxide ligand experience the largest change in length with 0.06−0.10 and 0.23−0.29 Å, respectively (Table 1). The pronounced shortening of the latter Fe−O bond is caused by the emergence of a charge on the ligand. The Fe−O bond lengths of 1.83−1.85 and 2.08−2.12 Å agree well with those reported for other octahedral high-spin iron(III) hydroxide[23,36,47] and iron(II) aqua[37,48,49] complexes, validating the assignments as a hydroxide and a water ligand in **1** and **2**, respectively. The variations in bond length and charge arising at the two oxygen donor ligands affect the hydrogen bonding interaction considerably; the significantly shorter interatomic distance O(1)···O(3) as well as the larger O(1)−H(3A)−O(3) angle indicate the presence of a substantially stronger hydrogen bonding interaction in **2** compared to **1**. Both aspects, the rather long axial Fe−N_{amine} bonds as well as the

https://doi.org/10.1021/jacs.1c04422
J. Am. Chem. Soc. 2021, 143, 13145−13155

increase in the strength of the hydrogen bonding interaction, contribute to the driving force of **1** to act as a reagent for H atom abstraction reactions. In **3**, the benzoate ligand is coordinated in a bidentate chelating fashion to a high-spin iron(II) ion. The difference of 0.16 Å in length between both Fe−O bonds tends to indicate a more localized charge character within the carboxylate functional group.

Magnetic and Spectroscopic Characterizations of the Complexes in the Solid State. The magnetochemical, UV−vis−NIR, and Mößbauer spectroscopic characterizations of solid **1** and **2** support the assignment of high-spin states to the iron ions. Temperature-dependent measurements of the magnetic susceptibility χ reveal χT-values of 4.61 and 3.61 cm^3Kmol^{-1} at 298 K for the ferric and the ferrous complex, respectively (Figure S13). Furthermore, the solids retain their high-spin states over the entire temperature range from 2 to 300 K. In addition, only very weak absorptions are observed in the vis−NIR spectrum of the solid ferric compound **1** (Figure S15), which is consistent with the sextet spin state. In contrast, the spectrum of the solid ferrous compound **2** (Figure S15) displays two d−d bands at 736 and 1370 nm, which arise from the splitting of the ^5E_g excited state in O_h symmetry to two states $^5A_{1g}$ and $^5B_{1g}$ (assuming idealized D_{4h} local symmetry). This finding is mainly attributed to the structural distortions imposed by the coordinated macrocyclic ligand such as the very elongated axial Fe−N_{amine} bonds. The solid-state spectrum of the ferrous compound **3** (Figure S15) with two d−d bands at ∼891 and ∼1307 nm is distinct from that of **2**. The decrease in energetic separation of the two d−d transitions from 6300 to 3570 cm^{-1} indicates that the difference in ligand field strength between the axial and the equatorial ligands is reduced in **3**. Mößbauer spectroscopy was applied to verify both the spin state and the oxidation state in complexes **1** and **2** (Figure S9). The ferric complex showed an asymmetric doublet with an isomeric shift (δ_{IS}) of 0.42 mm/s and a quadrupole splitting (ΔE_Q) of 2.25 mm/s (90 K). The ferrous complex showed a doublet with δ_{IS} = 1.04 mm/s and ΔE_Q = 2.63 mm/s (295 K). The decrease in δ_{IS} is consistent with a reduced electron shielding in the ferric compound as opposed to the ferrous compound, and the values for δ_{IS} are in line with the Mößbauer data of other iron complexes.[50] The unusually high quadrupole splitting in the ferric complex is explained by the pronounced differences in bond strength between the axial amine ligands and the equatorial ligands imposed on the complex by the distorting coordination properties of the macrocyclic ligand.[45] This substantial reduction in symmetry of the ligand field results in a high electric field gradient at the only seemingly totally symmetric high-spin d^5 shell of the high-spin iron(III) ion. In our study, Mössbauer spectroscopy also proved to be a very valuable tool for detecting small contaminations by the iron(II) starting complex in the attempted preparation of pure **1** by oxidation of **2** with molecular oxygen.

Depending on the substance investigated (**1a**, **1b**, or **1c**), the ATR-IR spectrum of **1** displays a feature between 3289 and 3392 cm^{-1} (Figure S7). On the basis of the shift in energy of the vibration to 2470 cm^{-1} upon H/D isotope substitution, the vibration can be unambiguously assigned to the O−H stretching vibration (Figure S8). The extent of decrease in energy of this vibration compared to the value of an unperturbed free hydroxide in the gas phase (3700−3570 cm^{-1})[51] is a measure of the binding strength of the hydroxide ligand to the metal ion as well as of the extent of involvement of the hydroxide ligand in hydrogen bonding interactions. Similar O−H vibrational energies have been observed for other iron(III) hydroxide complexes.[20,23] For the iron(II) aqua complex, two distinct O−H stretching vibrations are expected. However, only a single O−H stretching vibration between 3575 and 3338 cm^{-1} (**2a**−**c**) is observed (Figure S7). Deuterium substitution experiments of **2a** proved very helpful in identifying the weaker and broader second vibration (Figure S8). Thus, two features at 2490 and 2192 cm^{-1} are detected for the deuterated sample **2d** as compared to one feature at 3345 cm^{-1} in **2a**. Using the same ratio for the changes of vibrational energies due to the H/D substitution effect, the second vibration is calculated to occur at 2944 cm^{-1} for the H-substituted complex **2a** and is, therefore, obscured by the C−H vibrations detected in this energy range. The vibrations at 3345 and 2944 cm^{-1} are assigned to the individual O−H bonds involved in *inter*molecular and *intra*molecular hydrogen bonding interaction, respectively.

Characterization of the Complexes in Solution. The spin state and coordination environment of the iron(III) complex **1** are preserved in solution. Thus, the visible range of the electronic absorption spectrum is devoid of any features with intensities usually displayed by spin-allowed d−d transitions, and the EPR spectrum of a frozen solution of complex **1** in dimethylformamide (DMF) containing 0.2 mol·L^{-1} tetrabutylammonium perchlorate (TBAP) displays a rhombic signal that arises from an S = 5/2 species with real g-values of 1.999, 1.997, and 1.995, a zero-field splitting constant D of +2.75 cm^{-1}, and a rhombicity E/D of 0.107 (Figures 2, S10, and S11) as defined by the spin Hamiltonian described by eq 1 (with μ_B = Bohr magneton).

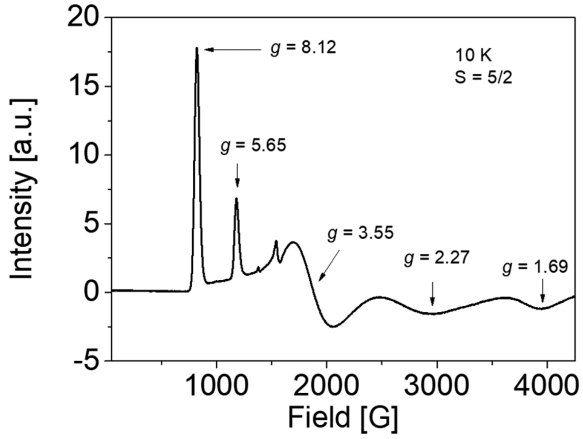

Figure 2. X-band EPR spectrum (9.3452 GHz) of a frozen solution of **1** in DMF containing 0.2 mol·L^{-1} TBAP at 10 K. Effective g-values are indicated. Some very minor paramagnetic contaminants are found at g_{eff} = 4.84 and g_{eff} = 4.28. The latter is commonly observed for ferric samples. More details, temperature-dependent spectra, and simulations can be found in the Supporting Information.

The rhombicity matches the low symmetry of the iron(III) site. A zero-field splitting constant D of similar size is obtained by fitting the magnetic susceptibility data of solid **1** assuming an isotropic g-value (D = +3.23 cm^{-1}).

$$\hat{H} = \mu_B \mathbf{B}^T \mathbf{g} \hat{\mathbf{S}} + D\left[\hat{S}_z^2 - \frac{S(S+1)}{3}\right] + E[\hat{S}_x^2 - \hat{S}_y^2] \quad (1)$$

https://doi.org/10.1021/jacs.1c04422
J. Am. Chem. Soc. 2021, 143, 13145−13155

ESI mass spectra of solutions of **1** in MeCN show a dominant signal at a m/z value of 546.3 (Figure S18). On the basis of the m/z value and its isotope pattern, this signal corresponds to the monocationic complex **1** (Figure S19), indicating the structural preservation of this species in solution. No signal arising from a μ-oxo bridged dinuclear complex can be detected. However, a considerably less intense second signal at m/z = 529.3 has been observed, which is attributed to the monocationic ferrous complex **3**. The strength of this signal varies substantially with the experimental conditions employed in the mass spectrometric investigation (Figure S20). Since we performed the mass spectrometric experiments only with analytically and spectroscopically pure compounds **1a** and **1c**, we attribute the observation of **3** to the partial loss of a hydroxyl radical from **1** under ESI-MS experimental conditions.

Solutions of both ferrous complexes **2** and **3** in MeCN render almost identical electronic absorption spectra with two absorption maxima observed at 732 and 1296 nm (Figures 3 and S15). The energetic separation of both maxima of 5945 cm^{-1} lies between those observed for the spectra of the solid complexes. In addition, the slightly asymmetric appearance of the absorption bands, especially that around 732 nm, points toward a superposition of two spectra most likely arising from cations **2** and **3**, respectively. A superposition of two spectral components with similar transitions as those observed for the solid complexes **2** and **3** can be confirmed by Gaussian curve analysis of the spectra of the dissolved complexes (Figure S16). These results suggest that an equilibrium between complexes **2** and **3** exists in the MeCN solutions.

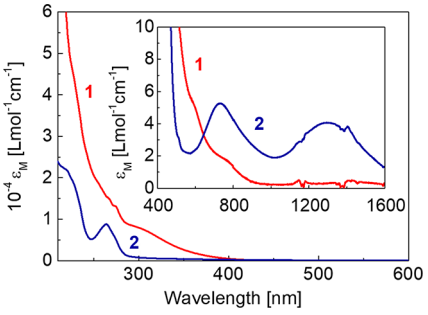

Figure 3. Electronic absorption spectra of **1** and **2** in acetonitrile solutions between 210 and 600 nm with a molar extinction coefficient ranging from 0 to 60 000 L $mol^{-1}cm^{-1}$ (main figure) and between 400 and 1600 nm with a molar extinction coefficient ranging from 0 to 10 L $mol^{-1}cm^{-1}$ (inset).

The ESI spectrum of dissolved complex **2** in MeCN reveals a dominant signal at m/z = 529.3 corresponding to **3** (Figures S18 and S19). No signal at m/z = 547.3 corresponding to the monocation **2** is detected. This shows that, under the experimental conditions of the ESI-mass spectrometric measurement, complex **2** easily loses its coordinated water molecule, rendering complex **3** during the transfer of cationic species into the gas phase.

The electrochemical properties of the complexes were investigated by cyclic voltammetry (Figure S17). At a scan rate of 100 mV/s, the cyclic voltammogram of complex **1** displays an irreversible reduction process at a peak potential $E_{p,red}$ of −366 mV vs SCE with a considerably less intensive first reoxidative current peak at $E_{p,ox}$ of −262 mV vs SCE. When both current peaks are attributed to the redox pair $[Fe^{III}(L\text{-}N_4{}^tBu_2)(OBz)(OH)]^+/[Fe^{II}(L\text{-}N_4{}^tBu_2)(OBz)(OH)]^0$ (**1**/**1**$^-$), a half-wave redox potential $E_{1/2}$ = −0.31 V vs SCE is calculated. A comparison of this redox potential to those of other (hydroxo)iron(III) complexes in acetonitrile solution is provided in Table S22. In contrast, the oxidation of a solution of **2** in MeCN occurs irreversibly at an oxidative peak potential $E_{p,ox}$ of 678 mV vs SCE.

To summarize the results presented up to this point, the structural aspects of the active site in rLOX, namely, the FeN_4O_2 immediate coordination environment and, particularly, the intramolecular hydrogen bonded *cis*-$[Fe^{III}(O_2CR)(OH)]^+$ and *cis*-$[Fe^{II}(O_2CR)(OH_2)]^+$ coordination units, are well reproduced in the ferric complex **1** and the ferrous complex **2**, respectively. In addition to the structural model qualities, the complexes display the same electronic properties as the enzyme. In our opinion, even complex **3** could prove itself to be an adequate model for an enzymatic state of lipoxygenase, which has not yet been explicitly demonstrated to exist for rLOX. In soybean LOX (sLOX), on the other hand, spectroscopic studies and EXAFS investigations reveal the existence of an equilibrium between a 5-coordinate and a 6-coordinate species in solution (40/60%), thus implying a dynamic coordination environment at the active iron(II) site when no substrate is present.[9,47,52] This observation is in line with the generally accepted role of carboxylate ligands in metalloproteins of providing easy access to a further open coordination site at a metal ion by switching from the bidentate chelating to the monodentate coordination mode.[53] Such an equilibrium also exists between model complexes **2** and **3**. Although the structural and electronic properties of the enzyme site are well reproduced by the presented complexes, the model complexes do not seem to match the redox properties of the enzyme. A considerably higher redox potential has been reported for the enzyme (+0.6 ± 0.1 V vs SHE for pH = 7−9).[54] The reason behind this discrepancy could be the slightly longer Fe−N and Fe−O bonds in the rLOX[7,8] and the extensive hydrogen bonding donor network provided by the protein environment around the active site of the enzyme.[2]

H Atom Abstractions from O−H Bonds. The functional model character was established by investigating the reactivity of the ferric complex **1** in abstracting H atoms from both O−H *and* C−H bonds of organic substrates. The reactions studied are displayed in Scheme 4.

Under anaerobic conditions at room temperature (RT), the reaction of **1** and 2,4,6-tri-*tert*-butylphenol (TTBP) resulted in the formation of the corresponding phenoxyl radical and the ferrous complex **2** within minutes (reaction II). The generation of the phenoxyl radical was unambiguously demonstrated by EPR spectroscopy (Figure S24) and by UV−vis spectroscopy (Figure S26). Moreover, the formation of the ferrous aqua complex **2** was deduced from the ESI mass spectrum of the reaction solution (Figure S21). The cationic mass spectrum reveals a species with an identical m/z value as the ferrous complex cation **3**, which in an earlier paragraph was described as also deriving from **2** under ESI-MS conditions. In addition, unreacted complex **1** was detected. The immutability of the ratio of intensities of the signals corresponding to **3** and **1** indicates that the reaction is not quantitative but instead leads to the constitution of an equilibrium. In order to determine the associated equilibrium constant K, a series of nine quantitative EPR experiments was carried out with varying initial concentrations of the reactants (Table S15, Figure S29). The

https://doi.org/10.1021/jacs.1c04422
J. Am. Chem. Soc. 2021, 143, 13145−13155

Scheme 4. Reactions of 1 with Organic Substrates Investigated for Establishing H Atom Abstraction from Suitable O−H (I−III) and C−H (IV−VI) Bonds

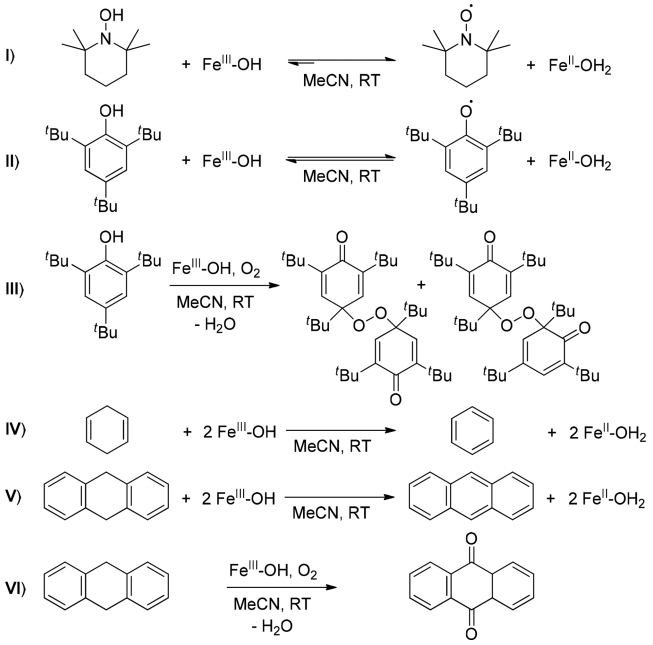

attainment of equilibrium conditions was ensured. Measurement of the EPR signal intensities allowed the determination of the equilibrium concentrations of the phenoxyl radical produced in each of the nine reactions starting with different initial concentrations of the educts. Using these values, the mean equilibrium constant K and the corresponding mean free reaction energy ΔG at 20 °C could be calculated to be K = 1.77 × 10^{-2} and ΔG = 2.35 kcal·mol^{-1} (estimated method error of ±0.14 kcal·mol^{-1}), respectively. Further experimental details are discussed in the Supporting Information. With the help of the reported bond dissociation free energy BDFE of TTBP in MeCN (74.8 kcal·mol^{-1}), the BDFE associated to the OH bond in **2** in MeCN is deduced to be 72.4 kcal·mol^{-1}.[55] A comparison to previously reported values for iron(II) complexes is presented in Table 2.

When one neglects the intrinsic difficulties in determining BDFE and the resulting uncertainties in comparing the values, the value determined in this study lies within the general range of values (68−84 kcal·mol^{-1}) observed for other iron(III) complexes capable of H atom abstraction. At the lower end of the range, there is the iron(II) complex $[Fe^{II}(H_2bim)_3]^{2+}$ possessing a N−H bond that participates in H atom transfer reactions. Iron(II) aqua complexes display O−H bonds with higher BDFE. The BDFE increases with the positive charge of the complex. Thus, the tetracationic low-spin iron(II) complex $[Fe^{II}(PyPz)(OH_2)_2]^{4+}$ with a *trans* FeN_4O_2 coordination environment containing a positively charged planar tetraaza-macrocyclic ligand exhibits the highest BDFE with 84 kcal·mol^{-1}. The BDFE is lowered somewhat in $[Fe^{II}(PY5)(OH_2)]^{2+}$ with a FeN_5O coordination environment arising from neutral ligands. Both monocationic complexes **2** and $[Fe^{II}(O^{Me2}N_4(tren))(OH_2)]^{+}$ possess a high-spin *cis*-$Fe^{II}N_4O_2$ coordination environment, but only in **2** is the aqua ligand involved in an intramolecular hydrogen bonding interaction. The presence of a hydrogen bonding interaction involving one of the O−H bonds of the coordinated water ligand and the carbonyl oxygen atom stabilizes the second O−H bond of the water ligand, resulting in an increase of its BDFE, and is, therefore, considered as an essential feature for the reactivity of the active site in the enzyme.[56] On the basis of the value for the BDFE of **2**, the reaction of **1** with 2,2,6,6-tetramethylpiperidin-1-ol (TEMPOH, reaction I) is expected to be almost quantitative, which could, accordingly, be verified by the experiment. It is noteworthy that, in contrast to **2**, the complex $[Fe^{II}(O^{Me2}N_4(tren))(OH_2)]^{+}$ reacts as a H atom donor with the TEMPO radical.

Table 2. Comparison of O−H and N−H Bond Dissociation Free Energies (BDFEs) of Various Iron(II) Complexes and Organic Substrates[a]

compound	solvent	BDFE [kcal·mol^{-1}]	reference
TTBP	MeCN	74.8	55
TEMPOH	MeCN	66	55
$[Fe^{II}(PyPz)(OH_2)_2]^{4+}$	H_2O	84	22
$[Fe^{II}(PY5)(OH_2)]^{2+}$	DMSO	80	20
$[Fe^{II}(L\text{-}N_4{}^tBu_2)(O_2CPh)(OH_2)]^{+}$	MeCN	72.4	this work
$[Fe^{II}(O^{Me2}N_4(tren))(OH_2)]^{+}$	MeCN	62.4[b]	57
$[Fe^{II}(H_2bim)_3]^{2+}$	MeCN	68.4	55

[a]PyPz = tetramethyl-2,3-pyridinoporphyrazine, PY5 = 2,6-bis(bis(2-pyridyl)methoxymethyl)pyridine, ($O^{Me2}N_4$(tren)) = 3-((2-(bis(2-aminoethyl)amino)ethyl)imino)2-methylbutan-2-olate, and H_2bim = 2,2′-bi-imidazoline. [b]The value in the original publication was determined to be 64.7 kcal·mol^{-1} using $C_{G,MeCN}$ = 54.9 kcal·mol^{-1}.[57] The value for $C_{G,MeCN}$ was later revised to be 52.6 kcal·mol^{-1}.[55] Employing the new value of $C_{G,MeCN}$, the BDFE(MeCN) for $[Fe^{II}(O^{Me2N4}(tren))(OH_2)]^{+}$ was recalculated. The structures of all referenced complexes are depicted in Scheme S3.[58]

Under aerobic conditions, complex **1** functions as a catalyst for the peroxidation of TTBP, rendering a mixture of 4,4′-peroxybis(2,4,6-tri(*tert*-butyl)-2,5-cyclohexadien-1-one) and its 2,4-isomer (reaction III) as shown by NMR spectroscopic and X-ray structure analytical investigations (see the Supporting Information for more details) of the crystalline material formed. The peroxidation of TTBP is assumed to proceed via a radical recombination step between two phenoxyl radicals and a triplet oxygen molecule. The catalyst **1** is regenerated under air as the ferrous complex **2** reacts readily with molecular oxygen (Figure S22).

H Atom Abstractions from C−H Bonds. To demonstrate the capability of a H atom abstraction from weak C−H bonds, anaerobic reactions of **1** with an excess of 1,4-cyclohexadiene (CHD) or 9,10-dihydroanthracene (DHA) were investigated at RT (reactions IV and V). Both CHD and DHA are frequently used substitute substrates for the 1,4-pentadiene unit of the fatty acid derivatives, which are the physiological substrates of the enzyme. H atom abstraction from C−H bonds by metal complexes with similar BDFE are known to occur, albeit at an approximately 10 000 times lower rate than that of O−H bonds.[59] Thus, even in the presence of a 10-fold excess of CHD, complete (>99%) conversion of the ferric complex to the ferrous complex at room temperature (RT) required 23 days under anaerobic conditions (Figure 4).

The ferrous product and benzene could be identified by ESI-MS (Figure S33) and NMR spectroscopy (Figure S35), respectively. Analogous studies with DHA yield a similarly slow reaction. The formation of anthracene in this reaction is also demonstrated by NMR spectroscopy (Figure S36). Under

https://doi.org/10.1021/jacs.1c04422
J. Am. Chem. Soc. 2021, 143, 13145−13155

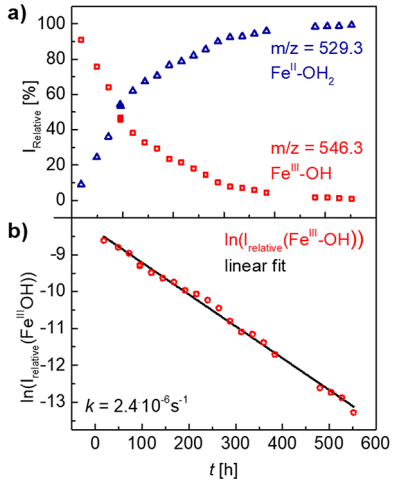

Figure 4. Reaction monitoring via ESI-MS by sampling the reaction solution on an almost daily basis (see the Supporting Information for further details). (a) Plot of the peak intensity I of the ESI mass signal versus the reaction time t for the reaction of **1** with CHD (initial concentrations c_0 (**1c**) = 2×10^{-4} mol·L^{-1} and c_0 (CHD) = 2×10^{-3} mol·L^{-1}). (b) Logarithmic plot of the intensity I versus reaction time t demonstrating first order kinetic properties. Experimental details are provided in the Supporting Information.

aerobic conditions in the presence of 20% of **1**, anthraquinone can be isolated at a yield of 87% (with respect to **1**) after 1 week. Under a pure oxygen atmosphere in the presence of 1% of **1**, yields of 53% can be achieved overnight (reaction VI), demonstrating that **1** acts as a radical initiator via H atom abstraction.

In preliminary reactivity experiments, the consumption of the ferric complex and the formation of the ferrous complex were followed by ESI-MS in the anaerobic reaction of **1** with a 10-fold excess of CHD at RT. An apparent pseudo-first order reaction kinetic was observed in these experiments (Figure 4). However, further, more carefully planned experiments are needed to determine reliable values for the kinetic parameters and the dependency of the rate constant on the substrate concentration. Nevertheless, the preliminary reactivity studies unambiguously demonstrate C−H abstraction reactivity of **1** with CHD as well as with DHA. The reactivity of **1** appears to be slower than that observed for $[Fe^{III}(PyPz)(OH)(OH_2)_2]^{4+}$ (in H_2O), $[Fe^{III}(Py5)(OH)]^{2+}$ (in MeCN), and $[Fe^{III}(H_2bim)_2(Hbim)]^{2+}$ (in MeCN).[20,22,60] Notably, in contrast to the observed C−H abstraction reactivity of the complex $[Fe^{III}(Py5)(OMe)]^{2+}$ in MeCN,[61] no reactivity could be observed for the ferric complex $[Fe^{III}(LN_4{}^tBu_2)(OMe)_2]^+$ (**4**) even with TTBP under the same experimental conditions, providing a strong argument for the special reactivity of the *cis*-(carboxylato)(hydroxo)iron(III) structural motif. There seem to be rate-enhancing cooperative effects caused by the hydrogen bonding interaction between the coordinated benzoate and hydroxide ligands. At the same time, the lack of reactivity of complex **4**, where the access to the lone pairs of the alcoholate ligands is sterically encumbered (see the Supporting Information for further details), rules out a simple, base-assisted oxidation mechanism of the substrate induced by prior dissociation of the basic ligand in solution. An overall H atom abstraction is the most likely occurring initial step in this model complex, similar to the mechanism proposed for lipoxygenases.

In our opinion, the special properties of the tetraazamacrocyclic ligand L-$N_4{}^tBu_2$ are also crucial to the reactivity of the ferric complex **1**. Thus, the usually highly favorable formation of μ-oxo-bridged diferric complexes is prevented by the steric hindrance caused by the bulky amine substituents of the ligand, ensuring the mononuclearity of the iron(III) site. In addition, rather long axial bonds are a trademark of the ligand, thus transferring less electron density from the ligand to the iron(III) ion and, thereby, raising the redox potential of the iron(III) site to some extent. Finally, the steric properties of the macrocyclic ligand do not prevent a potential substrate from reaching the hydroxo oxygen atom and reacting with it.

Theoretical Calculations. In order to probe if such a mechanistic scenario is viable, the initial C−H bond cleaving step was studied computationally. As a computational methodology, PW6B95-D3(BJ)/def2-TZVPP/SMD-(MeCN)//M06-L/def2-SVP/PCM(MeCN) was selected.[62] Subsequently, the transition states for C−H bond cleavage for the model substrates CHD and DHA were computed. The resulting barriers ($\Delta G^{\ddagger}_{298\ K}$) are 24.9 and 25.0 kcal·mol^{-1}, respectively, consistent with a reaction that occurs slowly at RT. With the computed reaction paths, not only was an overall H atom abstraction step confirmed to be mechanistically reasonable, but also, more interestingly, the exact nature of the C−H bond cleaving step could be determined. For reactions that follow a concerted proton-coupled electron transfer type (cPCET, alternative acronyms are EPT and CPET) mechanism,[63−67] two possible pathways can be differentiated: a H atom transfer (HAT), which is characterized by the transfer of a genuine H atom (electron and proton are transferred as a discrete entity) and, alternatively, a cPCET where the proton and electron are transferred separately.[68] For LOXs, a cPCET scenario has been well established.[2,14−16] Therefore, the electron flow along the intrinsic reaction coordinates (IRCs) of these reactions was studied using intrinsic bond orbitals (IBOs; Figure 5),[69,70] a methodology that has previously been shown to be capable of differentiating these scenarios.[71] For the oxidation of CHD, the C−H bond is found to be cleaved in a cPCET fashion. This can be seen in Figure 5b where the changes of the individual IBOs associated with the α-spin (i) and β-spin (ii) manifold of the C−H bond are shown. As the C−H bond is cleaved homolytically, the β IBO transforms into an Fe d-orbital and the α IBO remains with the derived organic radical in a continuous fashion; this finding is based on plotting the root square deviation of the partial charge changes of the studied IBOs (Figure 5a). This establishes the fate of the C−H bond and indicates that the electron transfer is decoupled from the proton transfer. If the lone pairs on the oxygen of the Fe^{III}−OH unit are inspected in an analogous way, the β-spin manifold reveals how a lone pair is transformed into an O−H bond, which corresponds to the proton transfer (Figure 5b, (iii)). Thus, it is concluded that both electron and proton transfers are indeed very much concerted. This is analogously observed for the oxidation of DHA (see the Supporting Information).

Therefore, the theoretical calculations establish that the model complex **1** not only is a structural and functional model of LOX but also mimics the event of C−H bond cleavage in the same fashion as LOX at an electronic structure level, which makes complex **1** a complete model.

https://doi.org/10.1021/jacs.1c04422
J. Am. Chem. Soc. 2021, 143, 13145−13155

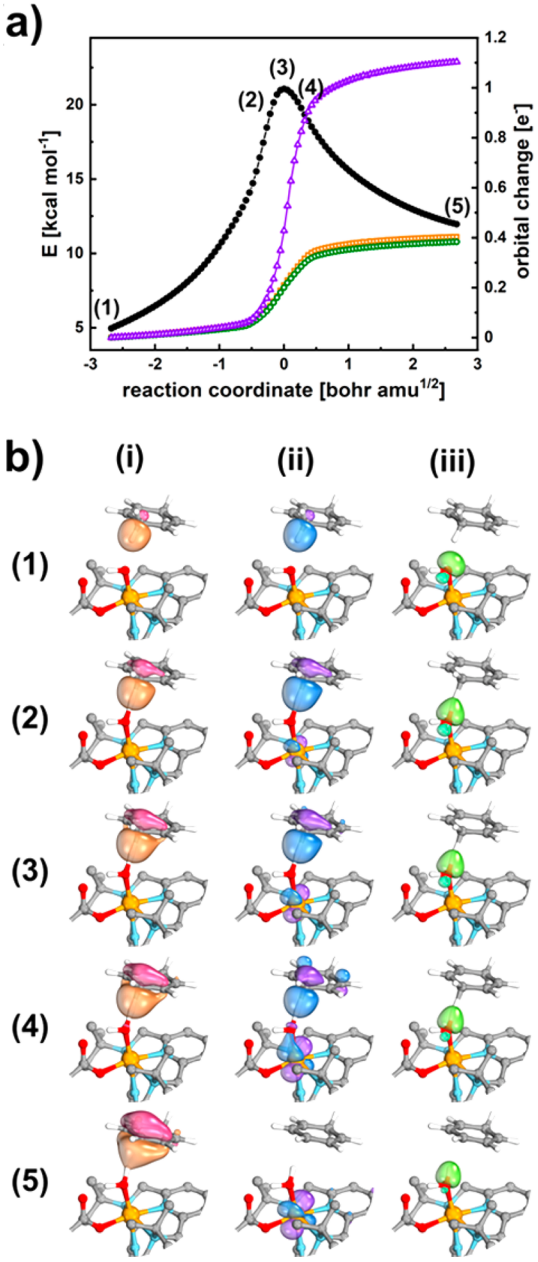

Figure 5. (a) Reaction plots of the orbital changes (e^-) along the IRCs for the C−H cleavage of CHD by complex **1**. Relative changes to the electronic energies are plotted in black circles, and changes to the IBOs are plotted separately for the α-spin (orange squares) and β-spin (purple triangles) manifolds of the C−H bond and the α-spin manifold of the lone pair on O (green circles). (b) Depiction of changes to IBOs relevant to C−H cleavage of CHD by complex **1** along the IRC. Localized orbitals are depicted for the α-spin (i) and β-spin (ii) manifolds of the C−H bond and the α IBO corresponding to the lone pair on O, resulting in the newly formed O−H bond (iii). All data were obtained at the M06-L/def2-SVP/CPCM level of theory.

CONCLUSION

In conclusion, here, we report on a structural as well as functional model for the active site in rLOX. Previous model studies have either succeeded in reproducing the structural and electronic aspects of the first coordination sphere of the oxidized active site, however, at the expense of losing reaction functionality,[23,24] or were able to provide an adequate functional model with very limited structural resemblance to the active site. The current study renders a model complex that reproduces all the relevant structural features of the first coordination shell of the active site in the oxidized state of rLOX, namely, the *cis*-FeN_4O_2 coordination environment and the *cis*-(carboxylato)(hydroxo)iron(III) coordination unit. Particularly noteworthy is the synthesis of both the corresponding *cis*-(carboxylato)(hydroxo)iron(III) and *cis*-(carboxylato)(aqua)iron(II) complexes as they represent models for the two enzymatic states observed in the catalytic cycle of LOX. The electronic properties of both complexes reflect those of the iron states in the enzyme. In addition, the (hydroxo)iron(III) complex shows reactivity in the overall H atom abstraction reaction with O−H and C−H bonds of suitable substrates, albeit with a lower rate than that observed for the enzyme. The BDFE of the O−H bond in the *cis*-(carboxylato)(aqua)iron(II) unit could be determined by quantitative EPR spectroscopic methods using the BDFE of the well-studied 2,4,6-tri(*tert*-butyl)phenol as a reference point. Theoretical calculations of the reactivity of the model complex indicate that the mechanism is consistent with the concerted proton-coupled electron transfer found in the enzyme. Furthermore, the ferric complex **1** can use its capability to abstract H atoms from weak O−H and C−H bonds in order to act as a catalyst in the aerobic peroxidation of TTBP and as a radical initiator in the oxidation of DHA to anthraquinone by air.

This investigation pursued the objectives of the synthetic analogue approach in bioinorganic studies to identify those intrinsic properties of the enzyme associated with the metal site and its first coordination sphere and those contributed by the protein matrix.[17] Very rarely, a synthetic analogue complex is a good model for the structural and/or electronic properties and, at the same time, a good model for the reactivity of an enzyme. The successful structural−functional modeling presented here indicates that the fundamental H atom abstraction reactivity of rLOX is derived from the *cis*-(carboxylato)(hydroxo)iron(III) coordination unit in an FeN_4O_2 ligand donor environment that is supplied by the protein matrix. Though the observation of a significantly slower reaction hints toward further protein matrix effects not captured by these simplified model complexes, this system offers a unique and advantageous opportunity for more detailed studies: specifically, how well-defined changes of structural and electronic factors at this coordination unit will influence its reactivity, a study that is hardly possible only with the enzyme.

ASSOCIATED CONTENT

Supporting Information

The Supporting Information is available free of charge at https://pubs.acs.org/doi/10.1021/jacs.1c04422.

Methods, synthetic and experimental procedures, supplementary figures and tables displaying characterization and structural analyses, theoretical calculations, and crystallographic information for **1a**, **1b**, **1c**, **2a**, **2b(1)**, **2b(2)**, **2c**, **3a**, **4a**, **4b**, and **6** (PDF)

Accession Codes

CCDC 2077026−2077036 contain the supplementary crystallographic data for this paper. These data can be obtained free of charge via www.ccdc.cam.ac.uk/data_request/cif, or by emailing data_request@ccdc.cam.ac.uk, or by contacting the

https://doi.org/10.1021/jacs.1c04422
J. Am. Chem. Soc. 2021, 143, 13145−13155

Cambridge Crystallographic Data Centre, 12 Union Road, Cambridge CB2 1EZ, UK; fax: + 44 1223 336033.

AUTHOR INFORMATION

Corresponding Author

Hans-Jörg Krüger − *Department of Chemistry, Technische Universität Kaiserslautern, 67663 Kaiserslautern, Germany;* orcid.org/0000-0002-8652-2154; Email: krueger@chemie.uni-kl.de

Authors

Emiel Dobbelaar − *Department of Chemistry, Technische Universität Kaiserslautern, 67663 Kaiserslautern, Germany;* orcid.org/0000-0002-5650-9231

Christian Rauber − *Department of Chemistry, Technische Universität Kaiserslautern, 67663 Kaiserslautern, Germany*

Thorsten Bonck − *Department of Chemistry, Technische Universität Kaiserslautern, 67663 Kaiserslautern, Germany*

Harald Kelm − *Department of Chemistry, Technische Universität Kaiserslautern, 67663 Kaiserslautern, Germany*

Markus Schmitz − *Department of Chemistry, Technische Universität Kaiserslautern, 67663 Kaiserslautern, Germany*

Matina Eloïse de Waal Malefijt − *Molecular Inorganic Chemistry, Stratingh Institute for Chemistry, Faculty of Science and Engineering, University of Groningen, 9747 AG Groningen, The Netherlands*

Johannes E. M. N. Klein − *Molecular Inorganic Chemistry, Stratingh Institute for Chemistry, Faculty of Science and Engineering, University of Groningen, 9747 AG Groningen, The Netherlands;* orcid.org/0000-0002-1290-597X

Complete contact information is available at: https://pubs.acs.org/10.1021/jacs.1c04422

Funding

H.-J.K. and E.D. would like to acknowledge financial support by the University of Kaiserslautern and funding supplied by the DFG (INST 248/266-1 FUGG).

Notes

The authors declare no competing financial interest.

ACKNOWLEDGMENTS

J.E.M.N.K. and M.E.d.W.M. would like to thank the Center for Information Technology of the University of Groningen for their support and for providing access to the Peregrine high-performance computing cluster. In addition, H.-J.K. and J.E.M.N.K. thank the COST Action CM1305 (ECOSTBio) for financial support to attend its conferences.

DEDICATION

Dedicated to the memory of Richard H. Holm.

REFERENCES

(1) Andreou, A.; Feussner, I. Lipoxygenases - Structure and reaction mechanism. *Phytochemistry* **2009**, *70* (13−14), 1504−1510.

(2) Gaffney, B. J. EPR Spectroscopic Studies of Lipoxygenases. *Chem. - Asian J.* **2020**, *15* (1), 42−50.

(3) Schilstra, M. J.; Veldink, G. A.; Vliegenthart, J. F. The dioxygenation rate in lipoxygenase catalysis is determined by the amount of iron (III) lipoxygenase in solution. *Biochemistry* **1994**, *33* (13), 3974−3979.

(4) Bryant, R. G.; Bailey, J. M.; Schewe, T.; Rapoport, S. M. Positional Specificity of a Reticulocyte Lipoxygenase. *J. Biol. Chem.* **1982**, *257* (257), 6050−6055.

(5) Kuhn, H.; Banthiya, S.; van Leyen, K. Mammalian lipoxygenases and their biological relevance. *Biochim. Biophys. Acta, Mol. Cell Biol. Lipids* **2015**, *1851* (4), 308−330.

(6) Xu, S.; Mueser, T. C.; Marnett, L. J.; Funk, M. O. Crystal structure of 12-lipoxygenase catalytic-domain-inhibitor complex identifies a substrate-binding channel for catalysis. *Structure* **2012**, *20* (9), 1490−1497.

(7) Gillmor, S. A.; Villasenor, A.; Fletterick, R.; Sigal, E.; Browner, M. F. The structure of mammalian 15-lipoxygenase reveals similarity to the lipases and determinants of substrate specificity. *Nat. Struct. Biol.* **1997**, *4* (12), 1003−1009.

(8) Choi, J.; Chon, J. K.; Kim, S.; Shin, W. Conformational flexibility in mammalian 15S-lipoxygenase: Reinterpretation of the crystallographic data. *Proteins: Struct., Funct., Genet.* **2008**, *70* (3), 1023−1032.

(9) Kuban, R. J.; Wiesner, R.; Rathman, J.; Veldink, G.; Nolting, H.; Solé, V. A.; Kühn, H. The iron ligand sphere geometry of mammalian 15-lipoxygenases. *Biochem. J.* **1998**, *332* (1), 237−242.

(10) Ivanov, I.; Kuhn, H.; Heydeck, D. Structural and functional biology of arachidonic acid 15-lipoxygenase-1 (ALOX15). *Gene* **2015**, *573* (1), 1−32.

(11) Newcomer, M. E.; Brash, A. R. The structural basis for specificity in lipoxygenase catalysis. *Protein science: a publication of the Protein Society* **2015**, *24* (3), 298−309.

(12) Navaratnam, S.; Feiters, M. C.; Al-Hakim, M.; Allen, J. C.; Veldink, G. A.; Vliegenthart, J. Iron environment in soybean lipoxygenase-1. *Biochim. Biophys. Acta, Protein Struct. Mol. Enzymol.* **1988**, *956* (1), 70−76.

(13) Goldsmith, C. R.; Jonas, R. T.; Stack, T. D. P. C-H bond activation by a ferric methoxide complex: modeling the rate-determining step in the mechanism of lipoxygenase. *J. Am. Chem. Soc.* **2002**, *124* (1), 83−96.

(14) Lehnert, N.; Solomon, E. I. Density-functional investigation on the mechanism of H-atom abstraction by lipoxygenase. *JBIC, J. Biol. Inorg. Chem.* **2003**, *8* (3), 294−305.

(15) Knapp, M. J.; Rickert, K.; Klinman, J. P. Temperature-dependent isotope effects in soybean lipoxygenase-1: correlating hydrogen tunneling with protein dynamics. *J. Am. Chem. Soc.* **2002**, *124* (15), 3865−3874.

(16) Li, P.; Soudackov, A. V.; Hammes-Schiffer, S. Impact of Mutations on the Binding Pocket of Soybean Lipoxygenase: Implications for Proton-Coupled Electron Transfer. *J. Phys. Chem. Lett.* **2018**, *9* (22), 6444−6449.

(17) Ibers, J. A.; Holm, R. H. Modeling coordination sites in metallobiomolecules. *Science (Washington, DC, U. S.)* **1980**, *209* (4453), 223−235.

(18) Holm, R. H.; Solomon, E. I. Preface: biomimetic inorganic chemistry. *Chem. Rev.* **2004**, *104* (2), 347−348.

(19) Majumdar, A.; Sarkar, S. Bioinorganic chemistry of molybdenum and tungsten enzymes: A structural−functional modeling approach. *Coord. Chem. Rev.* **2011**, *255* (9−10), 1039−1054.

(20) Goldsmith, C. R.; Stack, T. D. P. Hydrogen atom abstraction by a mononuclear ferric hydroxide complex: insights into the reactivity of lipoxygenase. *Inorg. Chem.* **2006**, *45* (15), 6048−6055.

(21) Mei, F.; Ou, C.; Wu, G.; Cao, Li; Han, F.; Meng, X.; Li, J.; Li, D.; Liao, Z. Non-heme iron(II/III) complexes that model the reactivity of lipoxygenase with a redox switch. *Dalton transactions* **2010**, *39* (18), 4267−4269.

(22) Gao, H.; Groves, J. T. Fast Hydrogen Atom Abstraction by a Hydroxo Iron(III) Porphyrazine. *J. Am. Chem. Soc.* **2017**, *139* (11), 3938−3941.

(23) Ogo, S.; Yamahara, R.; Roach, M.; Suenobu, T.; Aki, M.; Ogura, T.; Kitagawa, T.; Masuda, H.; Fukuzumi, S.; Watanabe, Y. Structural and spectroscopic features of a cis (hydroxo)-Fe(III)-(carboxylato) configuration as an active site model for lipoxygenases. *Inorg. Chem.* **2002**, *41* (21), 5513−5520.

(24) Ogo, S.; Wada, S.; Watanabe, Y.; Iwase, M.; Wada, A.; Harata, M.; Jitsukawa, K.; Masuda, H.; Einaga, H. Synthesis, Structure, and Spectroscopic Properties of $[Fe^{III}(tnpa)(OH)(PhCOO)]ClO_4$: A

Model Complex for an Active Form of Soybean Lipoxygenase-1. *Angew. Chem., Int. Ed.* **1998**, *37* (15), 2102−2104.
(25) Zaragoza, J. P. T.; Yosca, T. H.; Siegler, M. A.; Moënne-Loccoz, P.; Green, M. T.; Goldberg, D. P. Direct Observation of Oxygen Rebound with an Iron-Hydroxide Complex. *J. Am. Chem. Soc.* **2017**, *139* (39), 13640−13643.
(26) Ching, W.-M.; Zhou, A.; Klein, J. E. M. N.; Fan, R.; Knizia, G.; Cramer, C. J.; Guo, Y.; Que, L. Characterization of the Fleeting Hydroxoiron(III) Complex of the Pentadentate TMC-py Ligand. *Inorg. Chem.* **2017**, *56* (18), 11129−11140.
(27) Mukherjee, J.; Lucas, R. L.; Zart, M. K.; Powell, D. R.; Day, V. W.; Borovik, A. S. Synthesis, structure, and physical properties for a series of monomeric iron(III) hydroxo complexes with varying hydrogen-bond networks. *Inorg. Chem.* **2008**, *47* (13), 5780−5786.
(28) Bénisvy, L.; Halut, S.; Donnadieu, B.; Tuchagues, J.-P.; Chottard, J.-C.; Li, Y. Monomeric iron(II) hydroxo and iron(III) dihydroxo complexes stabilized by intermolecular hydrogen bonding. *Inorg. Chem.* **2006**, *45* (6), 2403−2405.
(29) Çelenligil-Çetin, R.; Paraskevopoulou, P.; Dinda, R.; Lalioti, N.; Sanakis, Y.; Rawashdeh, A. M.; Staples, R. J.; Sinn, E.; Stavropoulos, P. Oxidative Ligand Rearrangement Due to Incipient Aminyl Radicals in the Oxidation of Iron(II) Species with Dioxygen. *Eur. J. Inorg. Chem.* **2008**, *2008* (5), 673−677.
(30) Ortega-Villar, N.; Ugalde-Saldívar, V. M.; Flores-Pérez, B.; Flores-Alamo, M.; Real, J. A.; Moreno-Esparza, R. A new N6 hexadentate ligand and a novel heptacoordinated N_6O-type Fe(III) compounds: Synthesis, characterization and structure of $[Fe(dimpyen)(OH)](A)_2$ (A = PF_6^- or ClO_4^-). *Inorg. Chim. Acta* **2011**, *375* (1), 213−219.
(31) Yeh, C. Y.; Chang, C. J.; Nocera, D. G. "Hangman" porphyrins for the assembly of a model heme water channel. *J. Am. Chem. Soc.* **2001**, *123* (7), 1513−1514.
(32) Chambers, M. B.; Groysman, S.; Villagrán, D.; Nocera, D. G. Iron in a trigonal tris(alkoxide) ligand environment. *Inorg. Chem.* **2013**, *52* (6), 3159−3169.
(33) Burger, J.; Klüfers, P. Polyol-Metall-Komplexe. 17. Kristalline Eisen(III)-Komplexe mit zweifach deprotonierten Anhydroerythrit-Liganden. *Z. Anorg. Allg. Chem.* **1996**, *622* (10), 1740−1748.
(34) Hodges, K. D.; Wollmann, R. G.; Kessel, S. L.; Hendrickson, D. N.; van Derveer, D. G.; Barefield, E. K. Preparations and properties of nitrosyl complexes of iron tetramethylcyclam. X-ray structures of $[Fe(C_{14}H_{32}N_4)NO](BF_4)_2$, a S = 3/2−1/2 spin-equilibrium complex, and $[Fe(C_{14}H_{32}N_4)(NO)(OH)](ClO_4)_2{\cdot}CH_3CN$. *J. Am. Chem. Soc.* **1979**, *101* (4), 906−917.
(35) Drummond, M. J.; Ford, C. L.; Gray, D. L.; Popescu, C. V.; Fout, A. R. Radical Rebound Hydroxylation Versus H-Atom Transfer in Non-Heme Iron(III)-Hydroxo Complexes: Reactivity and Structural Differentiation. *J. Am. Chem. Soc.* **2019**, *141* (16), 6639−6650.
(36) Soo, H. S.; Komor, A. C.; Iavarone, A. T.; Chang, C. J. A hydrogen-bond facilitated cycle for oxygen reduction by an acid- and base-compatible iron platform. *Inorg. Chem.* **2009**, *48* (21), 10024−10035.
(37) Matson, E. M.; Bertke, J. A.; Fout, A. R. Isolation of iron(II) aqua and hydroxyl complexes featuring a tripodal H-bond donor and acceptor ligand. *Inorg. Chem.* **2014**, *53* (9), 4450−4458.
(38) Celenligil-Cetin, R.; Paraskevopoulou, P.; Dinda, R.; Staples, R. J.; Sinn, E.; Rath, N. P.; Stavropoulos, P. Synthesis, characterization, and reactivity of iron trisamidoamine complexes that undergo both metal- and ligand-centered oxidative transformations. *Inorg. Chem.* **2008**, *47* (3), 1165−1172.
(39) Yadav, V.; Gordon, J. B.; Siegler, M. A.; Goldberg, D. P. Dioxygen-Derived Nonheme Mononuclear FeIII(OH) Complex and Its Reactivity with Carbon Radicals. *J. Am. Chem. Soc.* **2019**, *141* (26), 10148−10153.
(40) Yadav, V.; Rodriguez, R. J.; Siegler, M. A.; Goldberg, D. P. Determining the Inherent Selectivity for Carbon Radical Hydroxylation versus Halogenation with $Fe^{III}(OH)(X)$ Complexes: Relevance to the Rebound Step in Non-heme Iron Halogenases. *J. Am. Chem. Soc.* **2020**, *142* (16), 7259−7264.
(41) Yadav, V.; Siegler, M. A.; Goldberg, D. P. Temperature-Dependent Reactivity of a Non-heme FeIII(OH)(SR) Complex: Relevance to Isopenicillin N Synthase. *J. Am. Chem. Soc.* **2021**, *143* (1), 46−52.
(42) Keshari, K.; Bera, M.; Velasco, L.; Munshi, S.; Gupta, G.; Moonshiram, D.; Paria, S. Characterization and reactivity study of non-heme high-valent iron−hydroxo complexes. *Chemical science* **2021**, *12* (12), 4418−4424.
(43) MacBeth, C. E.; Golombek, A. P.; Young, V. G.; Yang, C.; Kuczera, K.; Hendrich, M. P.; Borovik, A. S. O2 activation by nonheme iron complexes: A monomeric Fe(III)-Oxo complex derived from O2. *Science* **2000**, *289* (5481), 938−941.
(44) Cook, S. A.; Ziller, J. W.; Borovik, A. S. Iron(II) complexes supported by sulfonamido tripodal ligands: endogenous versus exogenous substrate oxidation. *Inorg. Chem.* **2014**, *53* (20), 11029−11035.
(45) Krüger, H.-J. Spin transition in octahedral metal complexes containing tetraazamacrocyclic ligands. *Coord. Chem. Rev.* **2009**, *253* (19−20), 2450−2459.
(46) Koch, W. O.; Krüger, H.-J. A Highly Reactive and Catalytically Active Model System for Intradiol-Cleaving Catechol Dioxygenases: Structure and Reactivity of Iron(III) Catecholate Complexes ofN,N′-Dimethyl-2,11-diaza[3.3](2,6)pyridinophane. *Angew. Chem., Int. Ed. Engl.* **1996**, *34* (2324), 2671−2674.
(47) Scarrow, R. C.; Trimitsis, M. G.; Buck, C. P.; Grove, G. N.; Cowling, R. A.; Nelson, M. J. X-ray spectroscopy of the iron site in soybean lipoxygenase-1: changes in coordination upon oxidation or addition of methanol. *Biochemistry* **1994**, *33* (50), 15023−15035.
(48) Becker, E.; Kirchner, K.; Mereiter, K. Hexaaqua-iron(II) bis-fac-tribromido-tricarbonyl-ferrate(II). *Acta Crystallogr., Sect. E: Struct. Rep. Online* **2009**, *65* (10), i71.
(49) Yahyaoui, S.; Rekik, W.; Naïli, H.; Mhiri, T.; Bataille, T. Synthesis, crystal structures, phase transition characterization and thermal decomposition of a new dabcodiium hexaaquairon(II) bis(sulfate): $(C_6H_{14}N_2)[Fe(H_2O)_6](SO_4)_2$. *J. Solid State Chem.* **2007**, *180* (12), 3560−3570.
(50) Gütlich, P.; Bill, E.; Trautwein, A. X. *Mössbauer spectroscopy and transition metal chemistry*; Springer: Heidelberg, 2011.
(51) Lutz, H. D.; Eckers, W.; Haeuseler, H. OH stretching frequencies of solid hydroxides and of free OH− ions. *J. Mol. Struct.* **1982**, *80*, 221−224.
(52) Pavlosky, M. A.; Zhang, Y.; Westre, T. E.; Gan, Q.-F.; Pavel, E. G.; Campochiaro, C.; Hedman, B.; Hodgson, K. O.; Solomon, E.I. Near-infrared circular dichroism and magnetic circular dichroism and x-ray absorption spectral comparison of the non-heme ferrous active sites of plant and mammalian 15-lipoxygenases. *J. Am. Chem. Soc.* **1995**, *117*, 4316−4327.
(53) Holm, R. H.; Kennepohl, P.; Solomon, E. I. Structural and Functional Aspects of Metal Sites in Biology. *Chem. Rev.* **1996**, *96*, 2239−2314.
(54) Nelson, M. J. Catecholate complexes of ferric soybean lipoxygenase 1. *Biochemistry* **1988**, *27*, 4273−4278.
(55) Wise, C. F.; Agarwal, R. G.; Mayer, J. M. Determining Proton-Coupled Standard Potentials and X-H Bond Dissociation Free Energies in Nonaqueous Solvents Using Open-Circuit Potential Measurements. *J. Am. Chem. Soc.* **2020**, *142* (24), 10681−10691.
(56) In general, a comparison with values reported in the literature turns out to be difficult because the respective BDFE values of the complexes depend decisively on the method used for their determinations. The most frequent method is the "Bordwell" analysis based on measuring the redox potentials and pK_a values of species involved in the proton-coupled electron transfer reaction of a metal complex, but here, experimental problems such as the frequent observation of irreversible electrochemical responses in cyclic voltammograms lead to less reliable data. The recently reported method of open-circuit potential measurement by J. M. Mayer seems to avoid these kinetic problems,[55] rendering thermodynamically more accurate data. In addition, the comparison of BDFE values obtained in different solvent, especially when the solvents differ substantially in

hydrogen bonding properties, is accompanied by a high degree of inaccuracy. Furthermore, errors in deriving constants used in the "Bordwell" analysis as well as confusion concerning the usage of BDFE versus BDE considerably complicate a reasonable comparison of values.
(57) Brines, L. M.; Coggins, M. K.; Poon, P. C. Y.; Toledo, S.; Kaminsky, W.; Kirk, M. L.; Kovacs, J. A. Water-soluble Fe(II)-H_2O complex with a weak O-H bond transfers a hydrogen atom via an observable monomeric Fe(III)-OH. *J. Am. Chem. Soc.* **2015**, *137* (6), 2253−2264.
(58) For a depiction of the structures, see the Supporting Information.
(59) Mayer, J. M. Understanding hydrogen atom transfer: from bond strengths to Marcus theory. *Acc. Chem. Res.* **2011**, *44* (1), 36−46.
(60) Roth, J. P.; Mayer, J. M. Hydrogen Transfer Reactivity of a Ferric Bi-imidazoline Complex That Models the Activity of Lipoxygenase Enzymes. *Inorg. Chem.* **1999**, *38* (12), 2760−2761.
(61) Jonas, R. T.; Stack, T. D. P. C−H Bond Activation by a Ferric Methoxide Complex: A Model for the Rate-Determining Step in the Mechanism of Lipoxygenase. *J. Am. Chem. Soc.* **1997**, *119* (36), 8566−8567.
(62) For a detailed description of the computational methods used and the corresponding references, see the Supporting Information. Here, we also provide a brief exploration of the reliability of the selected computational methodology.
(63) Hammes-Schiffer, S. Proton-Coupled Electron Transfer: Moving Together and Charging Forward. *J. Am. Chem. Soc.* **2015**, *137* (28), 8860−8871.
(64) Weinberg, D. R.; Gagliardi, C. J.; Hull, J. F.; Murphy, C. F.; Kent, C. A.; Westlake, B. C.; Paul, A.; Ess, D. H.; McCafferty, D. G.; Meyer, T. J. Proton-coupled electron transfer. *Chem. Rev.* **2012**, *112* (7), 4016−4093.
(65) Warren, J. J.; Tronic, T. A.; Mayer, J. M. Thermochemistry of proton-coupled electron transfer reagents and its implications. *Chem. Rev.* **2010**, *110* (12), 6961−7001.
(66) Huynh, M. H. V.; Meyer, T. J. Proton-coupled electron transfer. *Chem. Rev.* **2007**, *107* (11), 5004−5064.
(67) Mayer, J. M. Proton-coupled electron transfer: a reaction chemist's view. *Annu. Rev. Phys. Chem.* **2004**, *55*, 363−390.
(68) Usharani, D.; Lacy, D. C.; Borovik, A. S.; Shaik, S. Dichotomous hydrogen atom transfer vs proton-coupled electron transfer during activation of X-H bonds (X = C, N, O) by nonheme iron-oxo complexes of variable basicity. *J. Am. Chem. Soc.* **2013**, *135* (45), 17090−17104.
(69) Knizia, G. Intrinsic Atomic Orbitals: An Unbiased Bridge between Quantum Theory and Chemical Concepts. *J. Chem. Theory Comput.* **2013**, *9* (11), 4834−4843.
(70) Knizia, G.; Klein, J. E. M. N. Electron flow in reaction mechanisms–revealed from first principles. *Angew. Chem., Int. Ed.* **2015**, *54* (18), 5518−5522.
(71) Klein, J. E. M. N.; Knizia, G. cPCET versus HAT: A Direct Theoretical Method for Distinguishing X-H Bond-Activation Mechanisms. *Angew. Chem., Int. Ed.* **2018**, *57* (37), 11913−11917.

https://doi.org/10.1021/jacs.1c04422
J. Am. Chem. Soc. 2021, 143, 13145−13155